Applied Catalysis B: Environmental 110 (2011) 279–285

Contents lists available at SciVerse ScienceDirect

Applied Catalysis B: Environmental

journal homepage: www.elsevier.com/locate/apcatb

High surface area Au/CeO_2 catalysts for low temperature formaldehyde oxidation

Hong-Fang Li, Na Zhang, Ping Chen, Meng-Fei Luo, Ji-Qing Lu *

Key Laboratory of the Ministry of Education for Advanced Catalysis Materials, Institute of Physical Chemistry, Zhejiang Normal University, Jinhua 321004, China

ARTICLE INFO

Article history:
Received 18 July 2011
Received in revised form
11 September 2011
Accepted 12 September 2011
Available online 17 September 2011

Keywords:
Formaldehyde oxidation
Gold catalyst
CeO_2
High surface area
$Au_xCe_{1-x}O_{2-\delta}$ solid solution

ABSTRACT

Gold catalysts supported on high surface area CeO_2 were synthesized and tested for low temperature formaldehyde oxidation. It was found that the reactivity was greatly enhanced by increasing surface area of the support. Complete conversion of formaldehyde was obtained on a $3.0Au/CeO_2$-270 catalyst with a surface area of 270 $m^2\,g^{-1}$ at 50 °C, and a conversion of 92.3% was obtained at 37 °C over the same catalyst, which made it promising for indoor formaldehyde removal. Detailed characterizations of the catalyst showed that the enhancement could be attributed to two factors. One was that Au species mainly in high oxidation states formed on the high surface area CeO_2 resulted in a high degree of HCHO adsorption, as revealed by in situ diffuse reflectance infrared Fourier transform spectroscopy. The other was the high surface area CeO_2 provided more oxygen vacancies by the nano effect and the formation of $Au_xCe_{1-x}O_{2-\delta}$ solid solution as revealed by Raman spectroscopy, on which oxygen molecules could be transformed to active species for the reaction.

1. Introduction

Formaldehyde (HCHO) is a main volatile organic compound (VOC) emitted from the widely used constructive and decorative materials [1]. Long-term exposure to indoor air even containing very low concentration of HCHO may be detrimental to human health, resulting in diseases such as nasal and respiratory tract tumors [2]. Thus, great efforts have been made to reduce the indoor emission of HCHO for satisfying the stringent environmental regulations. Among the methods for formaldehyde abatement, oxidation of HCHO using heterogeneous catalysis appears to be a promising technology because of its higher efficiency compared to other methods such as absorbents [3], and more importantly, the resulting harmless products of CO_2 and H_2O.

Catalysts applied for HCHO oxidation include supported transition metals and noble metals. Transition metal catalysts for the reaction include Fe^{3+} modified 5A zeolites [4], Mn–Ce–O mixed oxides [5] and MnO_x [6–8]. Noble metal catalysts such as Ru, Pd and Pt could effectively convert HCHO at medium temperature [9–14]. It was also reported that complete conversion of HCHO was obtained over a Pt/TiO_2 catalyst even at room temperature [15]. Since the discovery of amazing catalytic properties in various reactions, supported gold catalysts were also found to be effective for formaldehyde oxidation [16–20]. The reactivities of the Au catalysts for the oxidation of formaldehyde are generally related to the support property, oxidation states of Au species and the synergy of the metal–support interface. In this respect, CeO_2 is a promising support for oxidation due to its unique properties such as fast oxygen storage/release and strong interaction between the metal and CeO_2. For example, Jia et al. [16] compared Au catalysts supported on TiO_2, CeO_2, and Ti–Ce–O mixed oxide for HCHO oxidation. It was found that the Au/CeO_2 showed the highest reactivity, which was due to a homogeneous dispersion of Au species on the support. Also, in our previous work, Au catalysts supported on SiO_2, Al_2O_3, TiO_2 and CeO_2 were investigated for formaldehyde oxidation and it was found that the Au/CeO_2 catalyst had the highest reactivity. The enhancement could be attributed to the stabilized cationic Au species on the CeO_2 surface and the oxygen activation promoted by CeO_2 [21]. Moreover, high surface area CeO_2 is favored for catalysis, as it can increase the dispersion of active components and consequently improve the stability and steady-state activity of the catalyst [22,23]. Zhang et al. [20] reported that three-dimensionally ordered macroporous (3DOM) Au/CeO_2 catalysts were much more active for HCHO oxidation than the powder Au/CeO_2 catalysts, due to the uniform macroporous structures leading to good distribution of catalytic species of Au nanoparticles with less aggregation. Furthermore, nano-scale CeO_2 crystallite can provide more active oxygen due to its down-size effect, which is beneficial to oxidation reaction [24,25].

For the purpose of indoor formaldehyde removal, highly active catalysts which could oxidize formaldehyde at low temperature (especially room temperature) are more desirable. Therefore, in this work, Au supported on CeO_2 with different surface areas were tested for formaldehyde oxidation, and it was found that

* Corresponding author. Tel.: +86 579 82287325; fax: +86 579 82282595.
E-mail address: jiqinglu@zjnu.cn (J.-Q. Lu).

0926-3373/$ – see front matter © 2011 Elsevier B.V. All rights reserved.
doi:10.1016/j.apcatb.2011.09.013

Table 1
Specific surface areas and Au contents of Au/CeO_2 catalysts.

Catalyst	Surface area ($m^2\ g^{-1}$)		Au content (wt.%)	
	Support	Catalyst	Nominal	Actual
$3.0Au/CeO_2$-270	270	261	5.0	3.0
$2.7Au/CeO_2$-150	150	143	5.0	2.7
$2.5Au/CeO_2$-37	37	34	5.0	2.5

the catalyst with high surface area could significantly enhance the reactivity. In addition, by various characterization techniques, a correlation between the catalyst structure and catalytic behavior was established.

2. Experimental

2.1. Catalyst preparation

High surface area CeO_2 was synthesized using a surfactant-templated method. Cerium nitride hexahydrate [$Ce(NO_3)_3{\cdot}6H_2O$, 99.9%] was used as the precursor and dodecyl sodium sulfate [$CH_3(CH_2)_{11}SO_4Na$), 99.0%] as the template. In a typical synthesis, the template (7.844 g, 27.2 mmol) was dissolved in deionized water (40 ml), and an aqueous solution (100 ml) of $Ce(NO_3)_3.6H_2O$ (4.342 g, 10 mmol) was drop-wise added with continuous stirring. The mixture was stirred for 30 min and then a solution (60 ml) of NaOH (99.5%, 1.7 g, 42.5 mmol) was added gradually. The formed precipitate was stirred at room temperature for another 24 h and then aged at 90 °C for 3 days. After that, the material was washed with large amount of deionized water. The light yellow material obtained was dried at 70 °C for 3 h in a vacuum oven, followed by calcination at 400 or 600 °C for 4 h, with a ramp of 3 °C min^{-1}. The resulting CeO_2 samples calcined at 400 and 600 °C had surface areas of 270 and 150 $m^2\ g^{-1}$, respectively.

Conventional CeO_2 was synthesized by a sol–gel method. An aqueous solution (100 ml) of $Ce(NO_3)_3{\cdot}6H_2O$ (4.342 g, 10 mmol) and citrate (99.5%, 1.82 g, 20 mmol) was heated at 90 °C under stirring until it became a viscous gel. Then the gel was dried at 120 °C overnight, and then calcined at 400 °C for 4 h to obtain the final material. The resulting CeO_2 sample had a surface area of 37 $m^2\ g^{-1}$.

Au/CeO_2 catalyst was prepared by a deposition–precipitation method (DP). In a typical synthesis, an aqueous solution of $HAuCl_4$ (100 ml, 1 $mg_{Au}\ ml^{-1}$) was heated to 70 °C and brought to pH ≈ 7 by the addition of 1 M NaOH solution, then 2.0 g of CeO_2 was added. After adjusting the suspension to pH ≈ 7, it was vigorously stirred at 70 °C for 1 h. The solid was then isolated by centrifugation and washed until free of chloride and dried at 70 °C for 3 h. After this, the catalyst was calcined at 300 °C for 4 h. The actual Au content of the final catalyst was analyzed by inductively coupled plasma (ICP) spectrometry. In designation, a *x*Au/CeO_2-*y* catalyst means that the gold loading is *x* wt.% and the surface area of the CeO_2 support is *y* $m^2\ g^{-1}$. The details of the gold catalysts were listed in Table 1.

2.2. Characterizations

Surface areas of the catalysts were determined by the modified BET method from the N_2 sorption isotherms at 77 K on an Autosorb-1 apparatus. The samples were heated at 373 K for 4 h under vacuum before measurement.

The actual Au content in the catalyst was determined by inductively coupled plasma (ICP) spectrometry.

X-ray diffraction (XRD) patterns were collected on a PANalytical X'Pert PRO powder diffractometer using CuKα radiation. The working voltage was 40 kV, and the current was 40 mA. The data were collected at 25 °C in a 2θ range of 20–130° with a scan rate of 1.2° min^{-1}. The microstructural parameters such as crystallite size and lattice parameter of the samples were determined by full curve fitting using a JADE 6.5 software.

Transmission electron microscopy (TEM) images of the catalysts were obtained on a JEM2010 microscope operated at 200 kV.

Raman measurements were performed on a Renishaw RM1000 with a confocal microprobe Raman system using a 514 nm (Ar^+ laser) laser as the excitation source with a dwell time of 20 s, number of scans of 2, and a resolution of 1 cm^{-1}.

Reducibility of the catalyst was measured by hydrogen temperature programmed reduction (H_2-TPR) technique. 50 mg of the sample was placed in a quartz reactor connected to a homemade TPR apparatus. The sample was heated in air at 100 °C for 1 h to remove water, and then cooled down to room temperature. Then the reactor was heated from 40 to 600 °C with a heating rate of 10 °C min^{-1} in a gas mixture (5% H_2 + 95% Ar, 30 ml min^{-1}). The amount of H_2 consumption was analyzed by a thermal conductivity detector (TCD).

X-ray photoelectron spectra (XPS) were recorded on a Kratos Axis Ultra DLD spectrometer using Al Kα radiation (1486.6 eV) as the excitation source. The analysis was performed at room temperature. Binding energies were calibrated by using the containment carbon (C 1s = 284.6 eV). Semi-quantitative analysis of atomic ratio was accomplished by determining the elemental peak areas.

Diffuse reflectance infrared Fourier transform (DRIFT) spectra of the samples were recorded using a Nicolet NEXUS 670 spectrometer equipped with an MCT detector and a DRIFTS cell (Harrick), under reaction conditions with a resolution of 4 cm^{-1}. An accumulation of 64 scans was used for collecting background and the sample spectra. About 30 mg of the ground catalyst was placed in the cell and pretreated at 100 °C for 0.5 h in a flow of He (40 ml min^{-1}) to remove water in the catalyst. Subsequently, the system was cooled to room temperature, and a background spectrum was recorded. Gaseous HCHO was generated by flowing N_2 (30 ml min^{-1}) through paraformaldehyde in a saturator kept at 50 °C. After the introduction of the gas mixture (500 ppm HCHO in N_2, 30 ml min^{-1}) for 15 min, the catalyst was purged with He (40 ml min^{-1}) to remove the physisorbed HCHO. Then, a spectrum was collected 5 min after the purge was finished.

2.3. Catalytic testing

The oxidation of HCHO was performed in a quartz tubular (i.d. = 6 mm) fixed-bed reactor under atmospheric pressure. 50 mg of catalyst in 40–60 mesh was loaded in the reactor. The reaction temperature was monitored by a thermocouple placed in the middle of the catalyst bed. A gas mixture containing 500 ppm HCHO and 20 vol.% O_2 balanced by N_2 was introduced as the reactants. Gaseous HCHO was generated by flowing 20% O_2 + 80% N_2 through paraformaldehyde in a saturator kept at 50 °C. The total flow rate was 100 ml min^{-1}, corresponding to a space velocity of 35,400 h^{-1}. The HCHO, and CO_2 were analyzed by an on-line GC (Shimadzu GC2014) equipped with a FID detector and two columns (carbon molecular sieve and TDX-502). The gaseous products passed through a methanization converter filled with Ni catalyst and all the carbon-containing products were converted to methane before they went to the FID detector to ensure a high intensity of signal.

Conversion of HCHO was calculated as follows:

$$\text{HCHO conversion}\,(\%) = \frac{[CO_2]_{out}\ \text{vol.\%}}{[HCHO]_{in}\ \text{vol.\%}} \times 100,$$

where $[CO_2]_{out}$ is the CO_2 concentration in the products (vol.%), $[HCHO]_{in}$ is the HCHO concentration in the feed gas (vol.%). Carbon balance is near 100%.

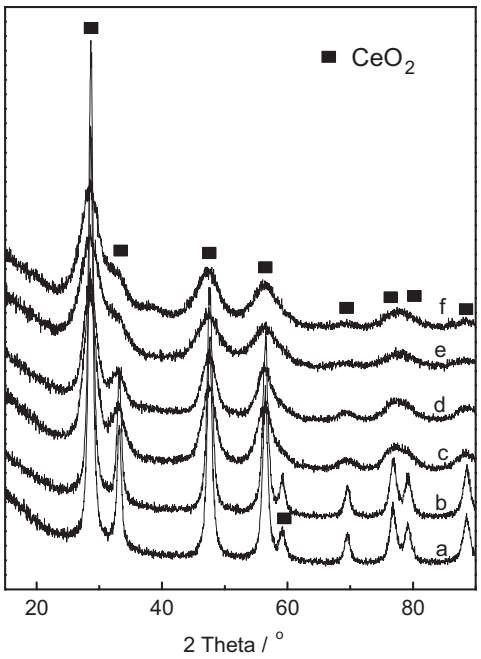

Fig. 1. XRD patterns of CeO_2 supports and Au/CeO_2 catalysts. (a) CeO_2-37; (b) $2.5Au/CeO_2$-37; (c) CeO_2-150; (d) $2.7Au/CeO_2$-150; (e) CeO_2-270; (f) $3.0Au/CeO_2$-270.

3. Results and discussion

Table 1 lists surface areas and actual Au loadings of the catalysts. It can be seen that the CeO_2 prepared by the template method offers much higher surface area than that by the sol–gel method. The template-assisted method has been employed to synthesize high surface area CeO_2 in literature, and the achievement of high surface area was due to the reduction of the surface tension by the interaction of Ce complex and surfactant during drying and calcination [26]. Also, the surface area decreases with elevated calcinations temperature, due to a sintering effect of the CeO_2 nanoparticles at high temperature. For the supported Au catalysts, it is found that the actual Au content in the catalyst is lower than the nominal value, due to the fact that the isoelectric point of CeO_2 (about 6) is lower than the preparation pH value (about 7). Moreover, the Au content on the high surface area support is slightly higher than that on the low surface area.

Fig. 1 presents the XRD patterns of the Au/CeO_2 catalysts, as well as the supports. It is clear that all these samples show typical cubic CeO_2 diffraction peaks (JCPDS 43-1002), without diffraction peaks due to Au species. The results indicate that Au species on the support are highly dispersed. Moreover, the intensities of the diffraction peaks become weaker with increasing surface area, suggesting a decline in the crystallite size of CeO_2. Detailed analysis of the XRD patterns using JADE 6.5 software gives lattice parameters and crystallite sizes of the samples, as shown in Table 2. It can be seen that the crystallite size of CeO_2 decreases from 9.8 to 2.0 nm as the surface area increases. Also, lattice parameter of the CeO_2 support becomes larger with increasing surface area, from 0.5423 nm for the CeO_2-270 sample to 0.5412 nm for the CeO_2-37. The increment in lattice parameter is due to more defect sites in the high surface area CeO_2, which may contain certain amount of Ce^{3+} with an ionic radius of 0.108 nm. Compared to the support, the Au/CeO_2 catalyst has relative smaller lattice parameter than the corresponding CeO_2 support, implying the incorporation of Au cations into the CeO_2 lattice since the ionic radius of Au^{3+} (0.085 nm) is smaller than that of Ce^{4+} (0.097 nm). For the $2.5Au/CeO_2$-37, no obvious change in lattice parameter is observed, probably due to the fact that few Au cations penetrate in the CeO_2 lattice.

Table 2
Lattice parameters and crystallite sizes of Au/CeO_2 catalysts.

Catalyst	S_{BET} ($m^2\ g^{-1}$)	Lattice parameter (nm)		Crystallite size of CeO_2 (nm)
		CeO_2	Au/CeO_2	
$3.0Au/CeO_2$-270	261	0.5423	0.5420	2.0
$2.7Au/CeO_2$-150	143	0.5420	0.5417	3.4
$2.5Au/CeO_2$-37	34	0.5412	0.5412	9.8

Fig. 2 shows the TEM images of the Au/CeO_2 catalysts. The identification of Au and CeO_2 is evidenced by *d*-spacing measurements, as shown in the figure. The Au particle sizes are in range of 2–4 nm, with those on the high surface area CeO_2 slightly smaller than those on the low surface area CeO_2. Also, the crystallinity of CeO_2 declines with increasing surface area, indicating the formation of defective sites on the nanoscale CeO_2 [27]. This is also in good agreement with the XRD results. Fig. 2d gives a low resolution image of the CeO_2-270 support, which illustrates that the material has no porous structure and consists of numerous small particles with a particle size of about 2 nm.

Fig. 3 shows the Raman spectra of the CeO_2 samples with different surface areas and the corresponding Au/CeO_2 catalysts. All these samples show one distinct band at 460 cm^{-1}, which could be attributed to F_{2g} mode vibration of CeO_2 [28]. For the high surface area CeO_2 (CeO_2-150 and CeO_2-270) and the corresponding Au/CeO_2 catalysts, one additional band at 590 cm^{-1} assigned to oxygen vacancies is observed [27,28]. Moreover, for the CeO_2 supports, with increasing surface area, the intensity of the band at 460 cm^{-1} is gradually weakened, and a red shift is observed. This suggests the CeO_2 particle size becomes smaller with increasing surface area [28], which is in consistent with the XRD results. For the Au/CeO_2 catalysts, the Raman spectra show similar features as the support. However, the intensities of the bands are relatively lower than those of the support, as the dark colored Au/CeO_2 catalysts strongly absorb excitation laser and scattering light, thus weakens the signal. As it is reported that oxygen vacancies play a very important role in oxidation reaction such as CO oxidaiton [29], the peak areas of the two bands are calculated (A_{590} and A_{460}) and the ratio of A_{590}/A_{460} reflects the relative concentration in the sample, as also shown in Fig. 3. It can be seen that the CeO_2-37 and the $2.5Au/CeO_2$-37 merely contains oxygen vacancies, probably due to the well crystallized CeO_2 support. For the high surface area CeO_2 and Au/CeO_2, oxygen vacancies are detected and the relative concentration increases with surface area. Meanwhile, the A_{590}/A_{460} ratio is larger for the Au/CeO_2 than the corresponding CeO_2 support, further indicating the incorporation of Au cations in the CeO_2 lattice to form a $Au_xCe_{1-x}O_{2-\delta}$ solid solution [30], which is again consistent with the XRD results.

Fig. 4 shows the H_2-TPR profiles of the Au/CeO_2 catalysts. The bare support CeO_2-37 shows a weak reduction peak at 500–550 °C. Comparatively, the Au catalysts show an additional low temperature reduction peak at about 140 °C, and two reduction peaks in high temperature range of 500–750 °C. The low temperature reduction peak could be assigned to the reduction of cationic Au species, and the high temperature peaks could be assigned to the reduction of surface and bulk CeO_2 [31]. It is worth noting that the low temperature reduction peak areas for the $2.7Au/CeO_2$-150 and the $3.0Au/CeO_2$-270 are higher than that for the $2.5Au/CeO_2$-37 catalyst, which is probably due to more cationic Au species in the former catalysts. Furthermore, the calibrated H_2 consumptions of the low temperature reduction peaks of the catalysts by a known amount of CuO powder are also listed in Fig. 4. These values are higher than the nominal H_2 consumption, suggesting a co-reduction of CeO_2

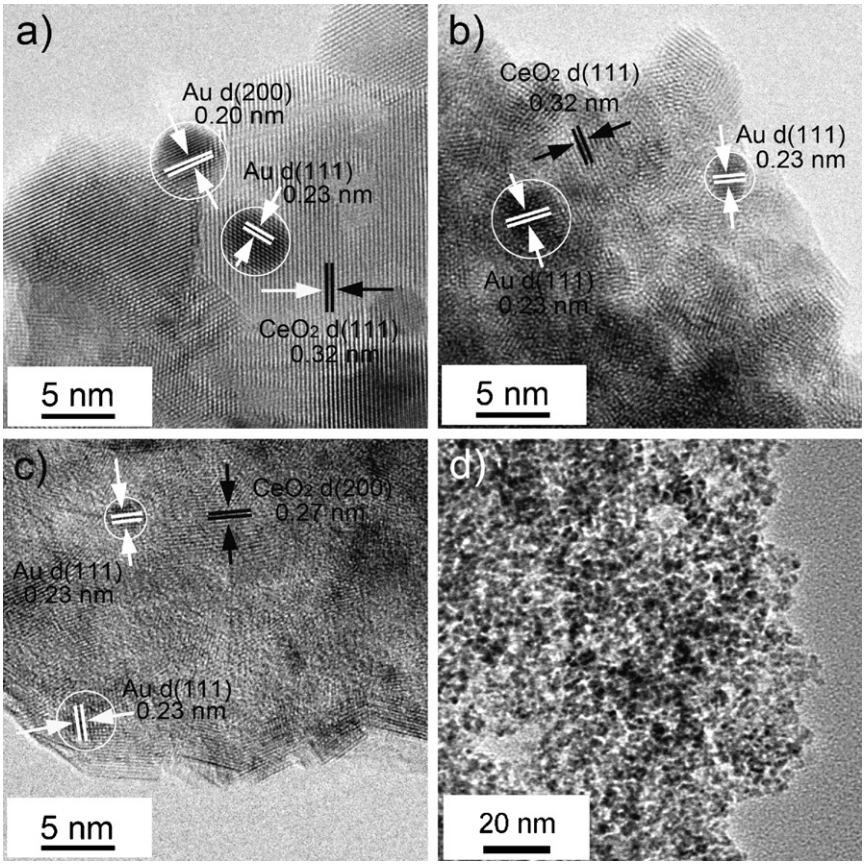

Fig. 2. HRTEM images of Au/CeO_2 catalysts. (a) $2.5Au/CeO_2$-37; (b) $2.7Au/CeO_2$-150; (c) $3.0Au/CeO_2$-270; (d) CeO_2-270.

resulting from a typical H_2 spillover effect [32]. Meanwhile, the deviation between the actual and nominal H_2 consumption is larger for the high surface area catalysts than for the low surface area one, implying an enhanced redox capability of the former catalysts.

In order to analyze the oxidation states of the Au species in the catalysts, XPS measurements were conducted and the results are shown in Fig. 5. The Au 4f core level spectra of the catalysts could be deconvoluted into several components and the results are listed in Table 3. The peaks in the ranges of 83.4–83.6, 84.4–84.5 and 85.1–85.4 eV could be assigned to Au^0, Au^+ and Au^{3+} species, respectively [33]. Also, the surface contents of these species in the catalysts differ with surface area. The content of low oxidation state

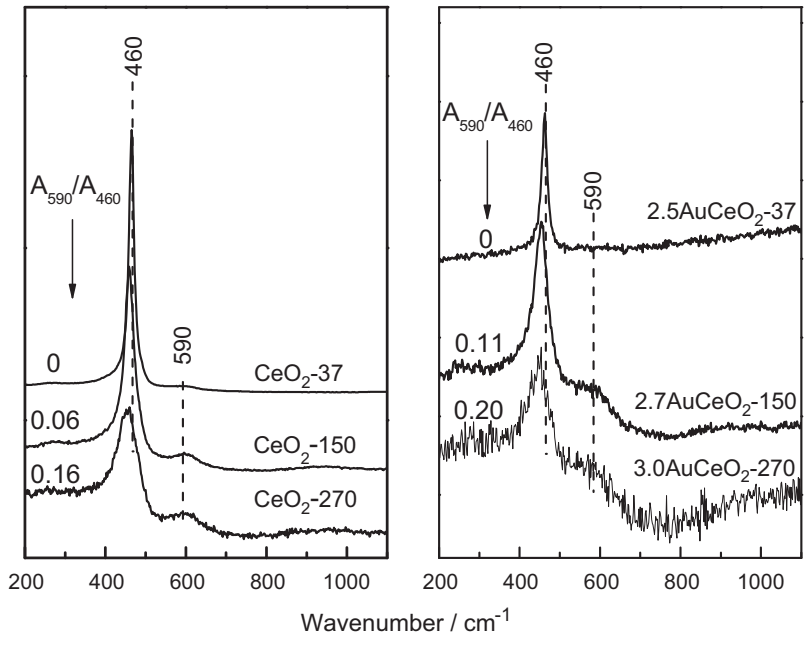

Fig. 3. Raman spectra of CeO_2 supports and Au/CeO_2 catalysts.

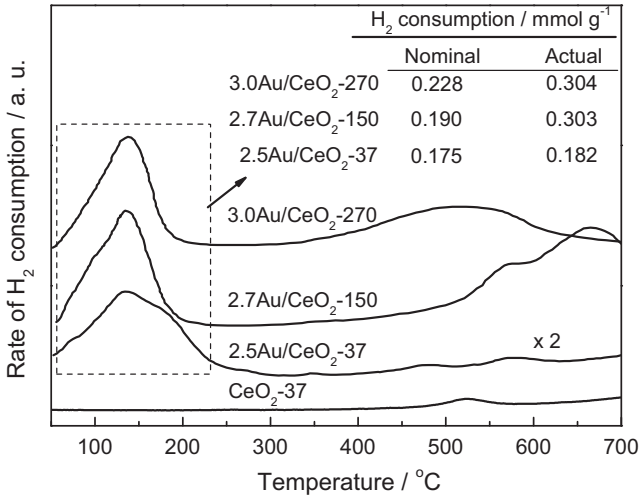

Fig. 4. H_2-TPR profiles of Au/CeO_2 catalysts. The nominal H_2 consumption is calculated based on the assumption that all the Au species in the catalysts are Au^{3+}.

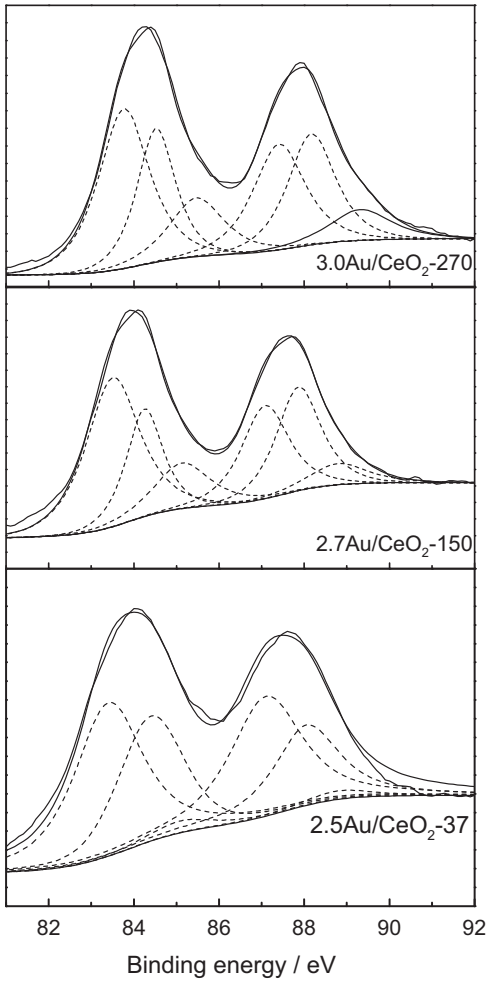

Fig. 5. Au 4f XPS spectra of Au/CeO_2 catalysts.

Table 3
XPS data analysis of Au/CeO_2 catalysts.

Catalyst	Peak position (eV)			Content (mol.%)		
	Au^0	Au^+	Au^{3+}	Au^0	Au^+	Au^{3+}
$2.5Au/CeO_2$-37	83.4	84.4	85.1	59	37	4
$2.7Au/CeO_2$-150	83.5	84.4	85.1	55	27	18
$3.0Au/CeO_2$-270	83.6	84.5	85.4	49	31	20

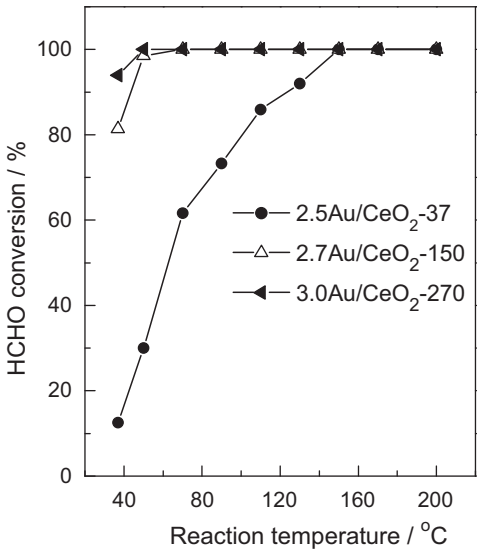

Fig. 6. Catalytic oxidation of HCHO over Au/CeO_2 catalysts Reaction conditions: C_{HCHO} = 500 ppm, O_2/N_2 (V/V) = 20/80, S.V. = 35,400 h^{-1}.

Au species (Au^0) decreases with increasing surface area, accompanied by a simultaneous increment in the content of high oxidation state Au species (Au^+ and Au^{3+}). The presence of the high oxidation state Au species may be related to the stabilization effect of nanosized CeO_2 particles on the cationic Au species through a strong interaction [34], as well as the formation of $Au_xCe_{1-x}O_{2-\delta}$ in the catalyst.

Fig. 6 presents the catalytic oxidation of formaldehyde over the catalysts. It can be seen that the high surface area catalysts are much more reactive compared to the low surface area catalyst. Complete conversions of HCHO are obtained on the $2.5Au/CeO_2$-37, $2.7Au/CeO_2$-150 and $3.0Au/CeO_2$-270 catalysts at 150, 70 and 50 °C, respectively. Furthermore, at reaction temperature of 37 °C, the $3.0Au/CeO_2$-270 and $2.7Au/CeO_2$-150 catalysts give HCHO conversions of 92.3% and 81.4%, respectively, while a HCHO conversion of 12.5% is obtained on the $2.5Au/CeO_2$-37 catalyst. This remarkable reactivity for the $3.0Au/CeO_2$-270 catalyst is among the highest values reported in literature [15–21], which makes it promising for low temperature HCHO oxidation.

In order to explain the significant enhancement of the reactivity obtained on the high surface area catalysts, in situ DRIFT spectra of HCHO adsorption on Au/CeO_2 catalysts at room temperature are recorded, as shown in Fig. 7. Bands at 1374, 1572, 2358 and 2842 cm^{-1} are observed on the $3.0Au/CeO_2$-270 catalyst. The bands at 1374 and 1572 cm^{-1} could be assigned to ν_s(COO)and ν_{as}(COO) of formate species [35], while the band at 2358 cm^{-1} could be assigned to gas phase CO_2 and the band at 2842 cm^{-1} could be assigned to ν(C–H). Similar features have been also observed on the $2.7Au/CeO_2$-150 catalyst, but with lower band intensities. For the $2.5Au/CeO_2$-37 catalyst, only a weak band at about 1580 cm^{-1} could be detected, which is assigned to the surface formate species. The DRIFT spectroscopic results clearly illustrate the different adsorption behaviors of HCHO over the catalysts. HCHO molecules could easily chemisorb on the $3.0Au/CeO_2$-270 and $2.7Au/CeO_2$-150 catalysts and convert to formate species and subsequently CO_2. However, HCHO molecules could hardly chemisorb on the low surface area catalyst ($2.5Au/CeO_2$-37) and thus makes the oxidation reaction difficult.

The above results indicate a significant promoting effect of CeO_2 support on the reactivity. This effect could be derived from the changes in the chemical properties of supported Au species and the CeO_2 support, because for oxidation reaction the catalytic behavior

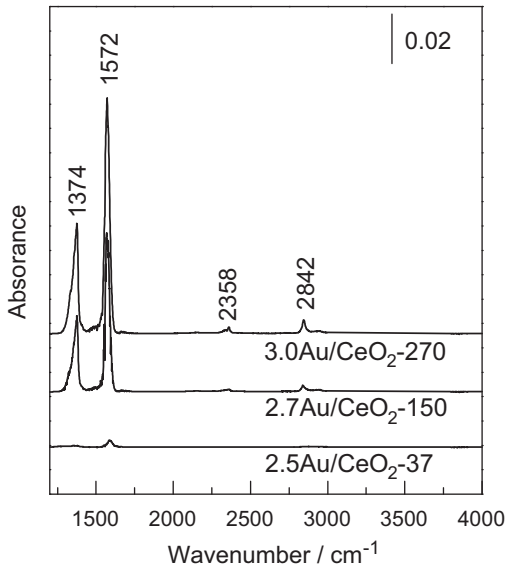

Fig. 7. In situ DRIFT spectra of HCHO adsorption on Au/CeO_2 catalysts at room temperature.

is related to the chemisorption and activation of the reactants on the catalyst surface, as well as the generation of active oxygen species. HRTEM results (Fig. 2) indicate that the CeO_2 supports hardly change the supported Au particle size but greatly alter the oxidation states of the Au species (as evidenced by XPS, Fig. 5). More cationic Au species are present in the high surface area catalysts, and the in situ DRIFT spectra of HCHO chemisorption (Fig. 7) suggest that HCHO molecules could strongly adsorb on the high surface area catalyst and produce formate species. The presence of formate species has been observed in both Pt [15] and Au [19] catalyst systems and regarded as the intermediates for the HCHO oxidation. As the chemisorption of HCHO takes place on the metal entities [15,19], the properties of the Au species should exert great impact on the chemisorption behavior, although the oxidation states of the Au species active for this reaction remain in argument. Zhang et al. [19] suggested that both Au^0 and Au^{3+} species in a Au/CeO_2 catalyst could adsorb HCHO molecules, while Li et al. [17] suggested that fractional charged Au species ($Au^{\delta+}$, $\delta < 1$) could be the active sites for formaldehyde oxidation over a gold/iron oxide catalyst. In the current work, regarding that the intensity of HCHO chemisorption on the $3.0Au/CeO_2$-270 catalyst is much higher than that on the$2.5Au/CeO_2$-37, it is reasonable to conclude that the HCHO molecules could chemisorb more strongly on the Au species in high oxidation states (Au^+ and Au^{3+}) than on those in low oxidation states (Au^0), since the $3.0Au/CeO_2$-270 contains more Au^+ and Au^{3+} species than the $2.5Au/CeO_2$-37. Note that the strong chemisorption may also be induced by the nanoscale CeO_2 support, as previous works already showed that Au supported on a nanosized CeO_2 resulted in a high degree of CO adsorption on Au particles located at the perimeter of the contact area between Au and the CeO_2 support and consequently a greatly enhanced reactivity for CO oxidation [34]. It is also worth noting that for CO oxidation over Au catalysts, surface carbonates or hydrocarbonates could be involved in the reaction pathways [36], however, in the present work, since these species are not observed in the DRIFT spectra (Fig. 7), it is more likely that the formate species instead of carbonate/hydrocarbonate species are the reaction intermediates for formaldehyde oxidation.

More importantly, the surface property of the CeO_2 must be considered because it may change dramatically with surface area. The nanosized CeO_2 contains much more defect sites than the large one and thus provides more oxygen vacancies that are able to adsorb and activate O_2 (e.g. superoxide O_2^-), as evidenced experimentally [29,37] and theoretically [38]. In the present work, Raman spectroscopic results (Fig. 3) reveal that the high surface area CeO_2 has a higher oxygen vacancy concentration compared to the low surface area CeO_2, implying a promoting effect of the generation of active oxygen species for the reaction. Interestingly, this promoting effect is even more pronounced with the addition of Au due to the formation of $Au_xCe_{1-x}O_{2-\delta}$ solid solution, as the Au/CeO_2 catalyst has a higher concentration of oxygen vacancy than the corresponding support. Meanwhile, as can be seen from the TPR results (Fig. 4) that the actual H_2 consumption is higher on the high surface area catalyst compared to that on the low surface area catalyst, indicating that the redox capability of the catalyst is enhanced by the defective CeO_2, which could also promote the reactivity.

Therefore, the enhanced reactivity obtained on the Au catalyst supported on high-surface area CeO_2 support could be attributed to two facts. One is that Au species (mainly in high oxidation states) formed on the high surface area CeO_2 may have a stronger interaction with the support, which could result in a higher degree of HCHO adsorption on Au particles. The other is the high surface area CeO_2 provides more oxygen vacancies by nanosize effect and the formation of $Au_xCe_{1-x}O_{2-\delta}$ solid solution, on which oxygen molecules could be transformed to active species for the reaction.

4. Conclusions

In this work, the effects of CeO_2 support on the reactivity of Au/CeO_2 catalysts for HCHO oxidation are investigated. It is found that the Au catalyst supported on high surface area CeO_2 is highly reactive for low temperature HCHO oxidation. The promoting effect of the CeO_2 support on the reactivity lies in the high oxidation states of Au species that provides centers for HCHO chemisorption; meanwhile, more oxygen vacancies are generated on the high surface area, on which oxygen molecules could be transformed to active species for the reaction.

Acknowledgement

This work was financially supported by Natural Science Foundation of Zhejiang Province (Grant No. Y407020).

References

[1] C. Yu, D. Crump, Build. Environ. 33 (1998) 357–374.
[2] J.J. Collins, R. Ness, R.W. Tyl, N. Krivanek, N.A. Esmen, T.A. Hall, Regul. Toxicol. Pharm. 34 (2001) 17–34.
[3] H. Nakayama, A. Hayashi, T. Eguchi, N. Nakamura, M. Tsuhako, Solid State Sci. 4 (2002) 1067–1070.
[4] X. Yang, Y. Shen, Z. Yuan, H. Zhu, J. Mol. Catal. A: Chem. 237 (2005) 224–231.
[5] X. Tang, Y. Li, X. Huang, Y. Xu, H. Zhu, J. Wang, W. Shen, Appl. Catal. B 62 (2006) 265–273.
[6] J.Q. Torres, J.M. Giraudon, J.F. Lamonier, Catal. Today (2011), doi:10.1016/j.cattod.2010.11.089.
[7] H. Tian, J. He, X. Zhang, L. Zhou, D. Wang, Microporous Mesoporous Mater. 138 (2011) 118–122.
[8] M.A. Sidheswaran, H. Destaillats, D.P. Sullivan, J. Larsen, W.J. Fisk, Appl. Catal. B: Environ. 107 (2011) 34–41.
[9] S. Imamura, Y. Uematsu, K. Utani, T. Ito, Ind. Eng. Chem. Res. 30 (1991) 18–21.
[10] K.T. Chuang, B. Zhou, S.M. Tong, Ind. Eng. Chem. Res. 33 (1994) 1680–1686.
[11] M.C. Álvarez-Galván, B. Pawelec, V.A. de la Peña O'Shea, J.L.G. Fierro, P.L. Arias, Appl. Catal. B: Environ. 51 (2004) 83–91.
[12] X. Tang, J. Chen, X. Huang, Y. Xu, W. Shen, Appl. Catal. B: Environ. 81 (2008) 115–121.
[13] N. An, Q. Yu, G. Liu, S. Li, M. Jia, W. Zhang, J. Hazard. Mater. 186 (2011) 1392–1397.
[14] J. Peng, S. Wang, Appl. Catal. B: Environ. 73 (2007) 282–291.
[15] C.B. Zhang, H. He, K. Tanaka, Catal. Commun. 6 (2005) 211–214.
[16] M. Jia, Y. Shen, C. Li, Z. Bao, S. Sheng, Catal. Lett. 99 (2005) 235–239.
[17] C.Y. Li, Y.N. Shen, M.L. Jia, S. Sheng, M.O. Adebajo, H. Zhu, Catal. Commun. 9 (2008) 355–361.

[18] Y. Shen, X. Yang, Y. Wang, Y. Zhang, H. Zhu, L. Gao, M. Jia, Appl. Catal. B: Environ. 79 (2008) 142–148.
[19] Y. Zhang, Y. Shen, X. Yang, S. Sheng, T. Wang, M.O. Adebajo, H. Zhu, J. Mol. Catal. A: Chem. 316 (2010) 100–105.
[20] J. Zhang, Y. Jin, C. Li, Y. Shen, L. Han, Z. Hua, X. Di, Z. Liu, Appl. Catal. B: Environ. 91 (2009) 11–20.
[21] H.F. Li, X.S. Liu, C.X. Guo, T. Liu, M.F. Luo, J.Q. Chin, J. Catal. 30 (2009) 1001–1006.
[22] E.S. Bickford, S. Velu, C.S. Song, Catal. Today 99 (2005) 347–358.
[23] S.Y. Lai, Y.F. Qiu, S.J. Wang, J. Catal. 237 (2006) 303–313.
[24] K.B. Zhou, X. Wang, X.M. Sun, Q. Peng, Y.D. Li, J. Catal. 229 (2005) 206–212.
[25] M.F. Luo, J.M. Ma, J.Q. Lu, Y.P. Song, Y.J. Wang, J. Catal. 246 (2007) 52–59.
[26] D. Terribile, A. Trovarelli, J. Llorca, C. Leitenburg, G. Dolcetti, J. Catal. 178 (1998) 299–308.
[27] X.M. Lin, L.P. Li, G.S. Li, W.H. Su, Mater. Chem. Phys. 69 (2001) 236–240.
[28] J.R. McBride, K.C. Hass, B.D. Poindexter, W.H. Weber, J. Appl. Phys. 76 (1994) 2435–2442.
[29] J. Guzman, S. Carrettin, J.C. Fierro-Gonzalez, Y. Hao, B.C. Gates, A. Corma, Angew. Chem. Int. Ed. 44 (2005) 4778–4781.
[30] A.M. Venezia, G. pantaleo, A. Longo, G.D. Carlo, M.P. Casaletto, F.L. Liotta, G. Deganello, J. Phys. Chem. B 109 (2005) 2821–2827.
[31] U.R. Pillai, S.S. Deevi, Appl. Catal. A: Gen. 299 (2006) 266–273.
[32] R. Kramer, M. Andre, J. Catal. 58 (1979) 287–295.
[33] Q. Fu, H. Saltsburg, M. Flytzani-Stephanopoulos, Science 301 (2003) 935–938.
[34] S. Carrettin, P. Concepción, A. Corma, J.M.L. Nieto, V.F. Puntes, Angew. Chem. Int. Ed. 43 (2004) 2538–2540.
[35] C. Zhang, H. He, K. Tanaka, Appl. Catal. B: Environ. 65 (2006) 37–43.
[36] S.T. Daniells, A.R. Overweg, M. Makkee, J.A. Moulijn, J. Catal. 230 (2005) 52–65.
[37] J. Guzman, S. Carrettin, A. Corma, J. Am. Chem. Soc. 127 (2005) 3286–3287.
[38] V. Shapovalov, H. Metiu, J. Catal. 245 (2007) 205–214.